PRECLINICAL AND CLINICAL SPECTROSCOPY – Note

Magnetic Resonance in Medicine 65:28–34 (2011)

Enhanced Neurochemical Profile of the Rat Brain Using In Vivo ^{1}H NMR Spectroscopy at 16.4 T

Sung-Tak Hong,[1] Dávid Zsolt Balla,[1] G. Shajan,[1] Changho Choi,[2] Kâmil Uğurbil,[1,3] and Rolf Pohmann[1]*

Single voxel magnetic resonance spectroscopy with ultrashort echo time was implemented at 16.4 T to enhance the neurochemical profile of the rat brain in vivo. A TE of 1.7 msec was achieved by sequence optimization and by using short-duration asymmetric pulses. Macromolecular signal components were parameterized individually and included in the quantitative analysis, replacing the use of a metabolite-nulled spectrum. Because of the high spectral dispersion, several signals close to the water line could be detected, and adjacent peaks could be resolved. All 20 metabolites detected in this study were quantified with Cramér-Rao lower bounds below 20%, implying reliable quantification accuracy. The signal of acetate was detected for the first time in rat brain in vivo with Cramér-Rao lower bounds of 16% and a concentration of 0.52 μmol/g. The absolute concentrations of most metabolites showed close agreement with values previously measured using in vivo ^{1}H NMR spectroscopy and in vitro biochemical assay. Magn Reson Med 65:28–34, 2011. ©2010 Wiley-Liss, Inc.

Key words: ^{1}H magnetic resonance spectroscopy (MRS); STEAM; ultrashort TE; LCModel; parameterization; macromolecular; ultrahigh-field

Localized in vivo ^{1}H NMR spectroscopy provides a unique opportunity for measuring brain metabolite concentrations noninvasively, thus providing neurochemical information of in vivo processes (1). This capability has been shown to benefit from increasing magnetic field strength because of gains in signal-to-noise ratio (SNR) and chemical shift resolution. These advantages were demonstrated by detecting and quantifying 18 metabolites in the rat brain in vivo with an ultrashort echo time stimulated echo acquisition mode (STEAM) sequence at 9.4 T (2). Subsequently, the detection of ascorbate (Asc) was reported with both ultrashort TE STEAM and a J-difference editing technique (3), also at 9.4 T. Recently, several signals adjacent to the water peak, including *N*-acetylaspartate (NAA) at 4.38 ppm, glycerophosphorylcholine (GPC) at 4.31 ppm, and phosphorylcholine (PCho) at 4.27 ppm, were resolved with narrow RF bandwidths for water suppression, taking advantage of the increased spectral dispersion at 14.1 T (4).

The availability of 16.4 T provides the potential of quantifying additional metabolites not detectable at lower field strength. Acetate (Ace), the anion of a short-chain organic acid, is widely recognized to be a substrate for glial cells (5). With in vivo ^{1}H NMR spectroscopy, the detection of the Ace methyl resonance at 1.9 ppm has not yet been possible due to its low concentration and virtually complete overlap with the methylene resonances of both γ-aminobutyric acid (GABA) at 1.889 ppm and *N*-acetylaspartylglutamate (NAAG) at 1.9 ppm. Detection of Ace has, therefore, been limited to ^{1}H-[^{13}C]-NMR spectroscopy (6) and high resolution ^{1}H-NMR on perchloric acid (PCA) extracts of the rat brain (7).

Although ultrashort TE makes it possible to obtain valuable metabolite information, it also leads to larger contributions from signals of macromolecules (MM); assessing this component is a critical factor in accurate metabolite quantification. Three different methods have been used to take account of the MM components in short TE in vivo ^{1}H NMR spectra. The first approach is to acquire an MM spectrum with an inversion-recovery metabolite-nulled measurement and then use this as a basis set in the quantification procedure (2). The second is to obtain both a metabolite spectrum and an MM spectrum from each study and subtract the MM spectrum from the metabolite spectrum before quantification (8). The third approach is to simulate MM components based on prior knowledge parameterized using a measured MM spectrum (9). Although the first method is the most widely used, the third approach is used in this study because of the advantage of allowing less constraints on the baseline by fitting each MM component or small groups of adjacent components separately (10), increasing the possibility to detect metabolites with very low concentrations, and to enable studies where MM concentrations vary due to pathologies.

In this work, the echo time of a STEAM sequence was minimized by reducing the duration of the slice-selective RF pulses and the spoiler gradients at a field strength of 16.4 T. This maximizes the SNR by minimizing signal decay due to T_2 relaxation and reduces J-modulation effects, resulting in improved accuracy of metabolite quantification as well as providing the feasibility of detecting metabolites previously unresolved in in vivo spectra. Therefore, the purpose of this study was (1) to provide an improved neurochemical profile of the rat brain in vivo with reasonable accuracy and (2) to

[1]High-Field Magnetic Resonance Center, Max-Planck Institute for Biological Cybernetics, 72076 Tübingen, Germany.

[2]Advanced Imaging Research Center, University of Texas Southwestern Medical Center, Dallas, Texas, USA.

[3]Center for Magnetic Resonance Research, University of Minnesota, Minneapolis, Minnesota, USA.

*Correspondence to: Rolf Pohmann, PhD, High-Field Magnetic Resonance Center, Max-Planck Institute for Biological Cybernetics, Spemannstrasse 41, 72076 Tübingen, Germany. E-mail: rolf.pohmann@tuebingen.mpg.de

Received 3 March 2010; revised 16 July 2010; accepted 27 July 2010.

DOI 10.1002/mrm.22609

Published online 6 October 2010 in Wiley Online Library (wileyonlinelibrary.com).

demonstrate the feasibility of simulated MM components to substitute the metabolite-nulled spectrum.

MATERIALS AND METHODS

Animal Handling

Twelve male Sprague-Dawley rats (204 ± 12 g) were used in the experiments. All rats experienced a 12 h alternating light-dark schedule in a temperature-controlled (23 ± 2°C) room with free access to food and water. Experiments were performed in accordance with the European guidelines for care and use of laboratory animals and with permission of the local review board.

Anesthesia was initially induced by inhalation of a mixture of O_2 and isoflurane at a 4–5% concentration and then maintained using 1.5–2.5% isoflurane. Rectal temperature was monitored and maintained at 37 ± 0.5°C by an electric heating pad placed under the torso.

In a supplementary measurement performed in one single rat, Ace was infused to ascertain the assignment of its methyl signal at 1.9 ppm. A three molar solution of Ace (adjusted to a pH of 7.0 with NaOH) was administrated through a tail vein at a variable rate over 2 h, using a protocol described previously (11).

Localized Proton Magnetic Resonance Spectroscopy

All measurements were performed on a 16.4 T/26 cm horizontal magnet (Magnex Scientific, Abingdon, UK) interfaced to a Bruker spectrometer (Bruker BioSpin GmbH, Ettlingen, Germany). The actively shielded gradient with 12 cm inner diameter has a maximum strength of 1000 mT/m and a rise time of 212 μsec. A home-built quadrature RF surface coil, composed of two geometrically decoupled single-turn coils (18 mm diameter), was used for both transmitting and receiving. The position of the volume-of-interest (VOI) was carefully selected based on multislice axial T_1-weighted MR images obtained using a rapid acquisition with relaxation enhancement (RARE) sequence (repetition time TR = 1500 msec, TE = 7.5 msec, slice thickness = 1.0 mm, matrix size = 256 × 256). A rectangular VOI (6.5 × 3.5 × 2.5 mm^3) was positioned in the thalamus of the rat brain. Localization was achieved with an ultrashort TE STEAM sequence (TR = 5000 msec, TM = 20 msec, TE = 1.7 msec, 256 averages, 2048 complex data points) consisting of three asymmetric 90° pulses (duration 700 μsec, bandwidth 7400 Hz) (12). The water signal was suppressed with the VAPOR (variable power RF pulses with optimized relaxation delays) technique, using seven chemical shift-selective gaussian RF pulses (9.1 msec, 300 Hz) interleaved with three outer volume saturation modules (12). To increase water suppression efficiency, an additional gaussian RF pulse was used in the TM period. Adjustment of all first- and second-order shim terms was accomplished with the fast automatic shimming technique by mapping along the projections (FASTMAP) (13), resulting in a total Creatine (tCr) linewidth of 23 ± 3 Hz (0.033 ppm) in vivo. For the Ace infusion experiment, TR was increased to 6000 msec and a 5.2 × 2.5 × 5.2 mm^3 voxel, mainly encompassing the hippocampus, was used.

For modeling the MM components, an inversion-recovery module was applied before the STEAM sequence, using an additional nonselective adiabatic full-passage pulse with a duration of 2 msec and a bandwidth of 11930 Hz. A sequence of metabolite-nulled spectra was measured with a TR of 2500 msec and inversion times (TI) of 660 msec, 710 msec, 730 msec, 770 msec, and 840 msec. These experiments consisted of 640 averages, except for the 710 msec measurement (1280 averages). The short TR in these experiments helped to further minimize contributions of residual metabolite signals by partially saturating them, while allowing the MM signals to recover completely because of their short T_1 relaxation times (14).

The short TE for all experiments was achieved using spoiler gradients with a duration of 431 μsec and a strength of 820 mT/m and 852 mT/m in the first and second half of the TE, respectively. The calculated diffusion weighting factor (b-value) was 64.1 s/mm^2, indicating negligible diffusion-induced signal loss for an apparent diffusion coefficient (ADC) on the order of 10^{-3} mm^2/s (15).

A reference spectrum composed of eight averages without water suppression was acquired before the actual measurement for eddy current correction (16).

Data Processing and Quantification

No postprocessing such as baseline correction, apodization, or water subtraction was applied to keep the original metabolite information.

Metabolite concentrations were analyzed with LCModel (17), using numerically calculated basis spectra generated with an in-house Matlab program (MathWorks, Natick, MA, USA), which uses the Liouville-von Neumann equation to calculate the evolution of the spin density matrix under the Hamiltonian with the actual parameters used in the STEAM sequence. Product-operator based transformation matrices for slice-selective 90° pulses were generated and used to calculate the density operator evolution over the sequence, including summation of density matrices over space (18,19). The spatial resolution for the simulation of slice selection was 1% of the slice thickness. The following 20 metabolites were included in the LCModel basis data: Ace, alanine (Ala), aspartate (Asp), Asc, creatine (Cr), GABA, glucose (Glc), glutamate (Glu), glutamine (Gln), Glycine (Gly), glutathione (GSH), GPC, PCho, myo-inositol (mI), lactate (Lac), NAA, NAAG, phosphocreatine (PCr), phosphorylethanolamine (PE), and taurine (Tau). All chemical-shift values and coupling constants were taken from (7) except for Asc (20), NAAG (21), and GABA (22). For absolute quantification, tCr was used as an internal reference, assumed to be 8.5 μmol/g (2).

MM signals were also included in the LCModel basis set. The necessary prior knowledge was obtained from the metabolite-nulled spectrum, by applying the Hankel Lanczos singular value decomposition (HLSVD) routine (23), built in jMRUI (24), to eliminate residual contributions from water and metabolite signals. LCModel parameters of MM signals were obtained from this spectrum and fine-adjusted based on the fitting result found with the metabolite-nulled spectrum to reach optimum agreement.

RESULTS

A representative in vivo ^{1}H NMR spectrum from the thalamus with fitting results is shown in Fig. 1. Compared to

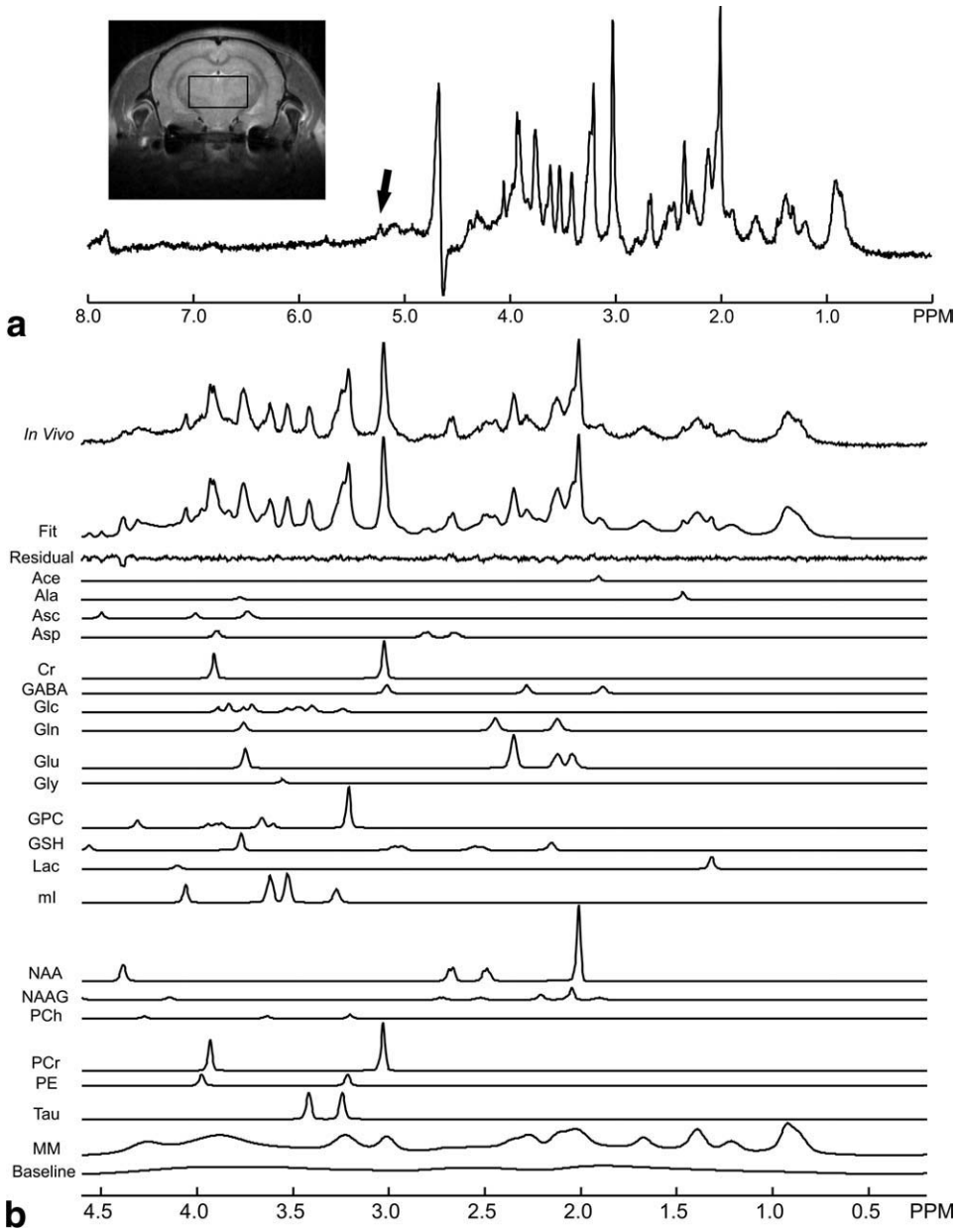

FIG. 1. **a**: Representative in vivo ^{1}H NMR spectrum from the thalamus of the rat brain acquired with ultrashort TE STEAM. The spectrum was processed only with eddy current correction, Fourier-transformation and phase correction; no apodization or baseline correction was applied. The Glc methine resonance at 5.22 ppm is marked by an arrow. **b**: Expanded region between 0.2 ppm and 4.6 ppm illustrating LCModel results with the basis set including both 20 metabolites and MM components. Shown are (from top to bottom) the in vivo spectrum, the fitted spectrum, the residual, fitting results of 20 individual metabolites, the MM components and the spline baseline. Note a partially saturated methine signal of NAA at 4.38 ppm owing to the water suppression pulses, resulting in a marked negative signal in the residual. All spectra in b are scaled identically.

the spectrum from 9.4 T (2), a clear separation was observable between two Glu methylene signals at 2.04 ppm and 2.11 ppm. All NAAG resonances including the glutamate moiety at 1.9 ppm and 4.14 ppm were clearly distinguishable. The separation of the GPC methylene signals at 3.603 ppm and 3.664 ppm was visible. Three metabolites, GPC at 4.314 ppm, PCho at 4.28 ppm, and NAA at 4.38 ppm, coresonating with MM, were clearly resolved.

The series of spectra acquired by inversion recovery measurements with different TI are shown in Fig. 2. In addition to a negative NAA peak at 2.02 ppm, two distinctly inverted peaks, tCr at 3.03 ppm and Tau at 3.246 ppm, are visible at a TI of 660 msec and, having already crossed the null point, at 730 msec (Fig 2a). A TI of 710 msec was found as optimum, yielding minimal contributions of NAA at 2.02 ppm as well as of Tau at 3.246 ppm and 3.422 ppm. HLSVD was applied to further eliminate the residual metabolite signals, NAA at 2.02 ppm and 2.68 ppm, Tau at 3.422 ppm and tCr at 3.94 ppm from this spectrum. The results of the parameterization of all MM components are summarized in Table 1. To model the complex structures between 2.0 ppm and 2.7 ppm and at around 3.8 ppm, signals M20 and M38 were composed of six and three single resonances with fixed amplitude ratios, respectively. The M09 signal was modeled by two overlapping components M09a and M09b that were fitted independently, yielding a good replication of its lineshape with minimum residual.

Remaining discrepancies between simulated and measured peaks, especially in the region of the M38 component, which could not be modeled satisfactorily by the Gaussian-Lorentzian lineshape generated by LCModel (25), are compensated by the elaborately regularized spline baseline obtained with a knot spacing of 0.15 in

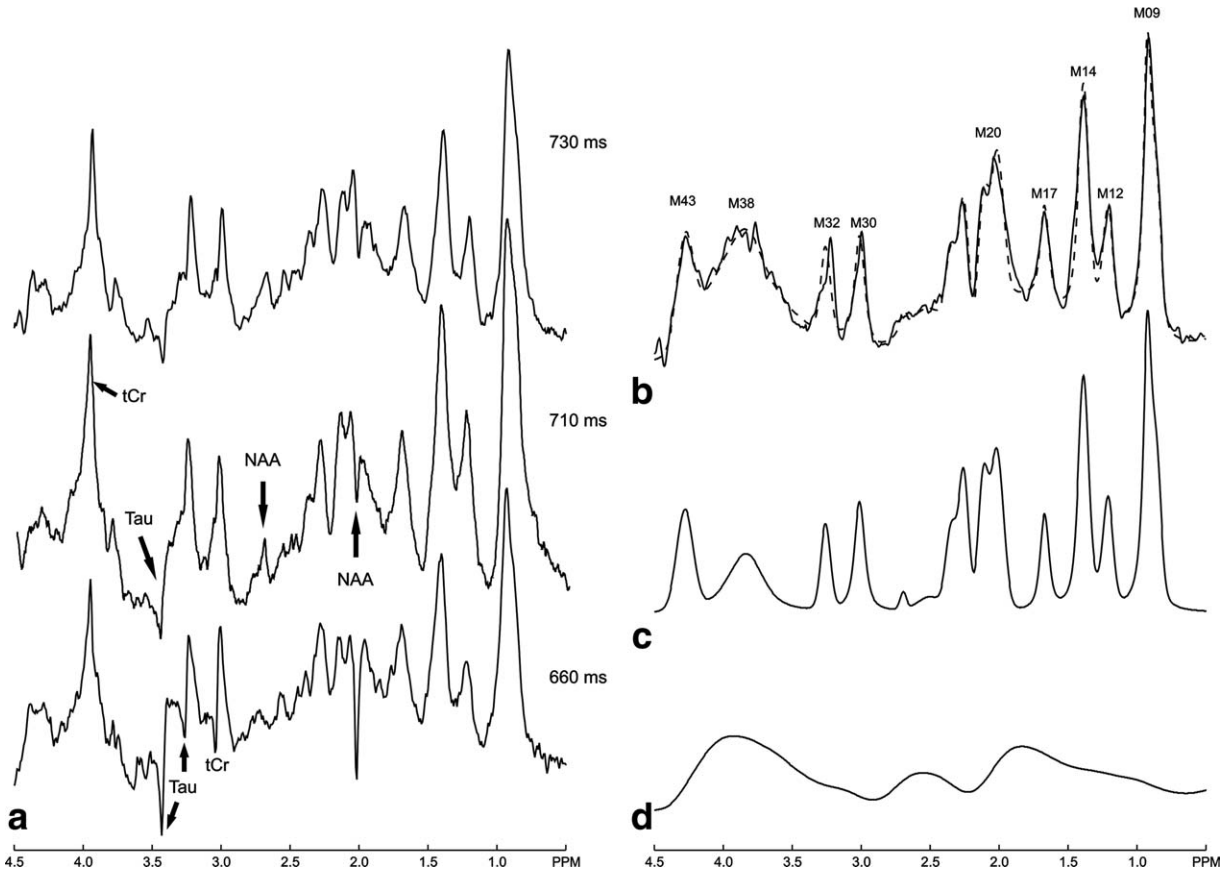

FIG. 2. **a**: Series of MM spectra with increasing TI. The tCr signal at 3.94 ppm is positive in all spectra due to its shorter T_1. The MM spectrum with a TI of 710 msec shows residual metabolite contributions, negative peaks of NAA at 2.02 ppm and Tau at 3.422 ppm, and positive peaks of NAA at 2.68 ppm and tCr at 3.94 ppm, marked with arrows. All spectra were treated with an exponential filter with a linebroadening of 20 Hz. **b**: Comparison of the LCModel fitting results obtained with the measured MM spectrum and the parameterized MM components (dashed line). Simulated MM spectrum (c) and spline baseline (d) as found by parameterization of the measured metabolite-nulled spectrum in LCModel. The dashed curve is the summation of the fitted MM components (c) and the spline baseline (d). All signals (b–d) are scaled equally.

LCModel. Adding this baseline to the fitted MM components shows close agreement between the fitted and the measured MM spectrum (Fig. 2b). Consistent and reliable determination of MM components is indicated by the low standard deviations and CRLBs (Table 1).

The fitting result of the LCModel analysis with the basis set including all 20 metabolites and MM components demonstrates the reliable determination of each individual metabolite and MM contributions reflected by the flat baseline (Fig. 1b). The high sensitivity and increased chemical dispersion make it possible to resolve metabolites with very low concentrations such as Ace resonating at 1.9 ppm and Gly at 3.55 ppm in all rats measured in this study.

Quantitative metabolite concentrations are summarized in Table 2, with and without including Ace and Gly in the basis set in the LCModel analysis. All analyzed metabolites demonstrate average CRLBs below 20%. The inclusion of Gly in the LCModel analysis had no influence on the quantification of the overlapping line of mI. NAAG, one of the overlapping metabolites with Ace, also shows a consistent concentration with and without including Ace in the basis data, whereas the concentration of GABA shows a slight change which may indicate a small dependence between these two signals. Figure 3 shows the residuals of LCModel analysis, with and without including Ace and Gly in the basis data. While the latter display distinct peaks at 1.9 ppm and at 3.55 ppm, these spurious signals disappear when including the two metabolites in the basis data. For Ace, the change in the fitted spectra leading to the disappearance of the residual peak when including Ace in the basis set is displayed in Fig. 3b (uppermost). The spectrum acquired with Ace infusion is presented in Fig. 3c, showing substantial increase of the Ace signal (1.39 μmol/g, CRLB 8%) with unchanged amplitudes of the overlapping two metabolites, GABA (1.03 μmol/g, CRLB 16%) and NAAG (0.99 μmol/g, CRLB 10%). Thus, only the Ace concentration was modified compared to the values measured without Ace infusion without affecting the methylene signals of GABA at 1.889 ppm and of NAAG at 1.9 ppm, which confirms the stable and independent detection of the Ace signal.

DISCUSSION

This study presents the first measurements of in vivo ^{1}H NMR spectra at 16.4 T, showing for the first time the possibility to detect Ace in the rat brain in vivo using

Table 1
Parameterization of Individual Macromolecular Components Derived from the Metabolite-Nulled Spectrum. Fitting Results in the LCModel Analysis Were Expressed with Relative Standard Deviation (SD) and CRLB

MM component[a]	Frequency (ppm)	Linewidth (ppm)	Amplitude (a.u.)	SD (%)[d]	CRLB (%)
M09[b]				18	9
M09a	0.86	0.10	3.2		
M09b	0.92	0.04	5.0		
M12	1.22	0.10	2.5	20	12
M14	1.41	0.08	4.0	10	7
M17	1.67	0.07	2.0	12	9
M20	2.05	0.12	1.9	18	7
	2.15	0.08	1.1		
	2.29	0.08	1.2		
	2.38	0.09	0.8		
	2.54	0.20	0.3		
	2.73	0.05	0.1		
M30	3.00	0.07	2.3	21	9
M32	3.20	0.10	2.5	16	10
M38	3.85	0.26	1.7	14	13
	3.82	0.15	1.2		
	3.77	0.15	0.9		
M43[c]	4.35	0.16	0.9		

[a]Labels assigned according to the resonance frequency in ppm. M20 and M38 are composed of six and three single components, respectively, and are labeled with the resonance frequency of the first component.
[b]M09a and M09b were quantified independently. As they form a single signal, the SD of their sum and their average CRLB are given.
[c]The fitting result was not determined as it was outside of the spectral range between 0.2 ppm to 4.3 ppm in the LCModel analysis.
[d]SD is expressed in percent of the mean.

ultrashort TE ^{1}H NMR spectroscopy. Acquisition and quantification of the extended neurochemical profile are achieved by taking advantage of the increased spectral dispersion and sensitivity at 16.4 T in combination with an improved LCModel basis set, containing both metabolite and MM information. The practical problems of high field, including the increased chemical shift displacement, the decreased T_2 relaxation time, and the high sensitivity to susceptibility effects, are compensated by using short-duration asymmetric pulses with a high bandwidth, by minimizing TE and by correcting the field inhomogeneities with FASTMAP.

The simulated MM components found by parameterization of the metabolite-nulled spectrum determined the underlying MM contributions of the data acquired with ultrashort TE. The simulated MM signals are able to accurately model the MM contributions to the spectra, as is demonstrated especially in the MM dominant region

Table 2
Comparison of Average Absolute Concentration (±SD) and Average CRLB Determined With (left column) and Without (right column) Including Ace and Gly in the LCModel Analysis. The Average SNR as Determined by LCModel Was 38 ± 3

Metabolites	Concentrations (μmol/g)	CRLB (%)	Concentrations (μmol/g)	CRLB (%)
Ace	0.52 ± 19%	16		
Ala	0.65 ± 21%	14	0.65 ± 22%	14
Asc	2.39 ± 9%	7	2.49 ± 9%	7
Asp	2.62 ± 15%	8	2.66 ± 16%	8
Cr	3.36 ± 9%	5	3.43 ± 8%	5
GABA	1.58 ± 16%	7	1.83 ± 13%	6
Glc	0.94 ± 24%	11	0.86 ± 25%	13
Gln	3.57 ± 13%	3	3.71 ± 14%	3
Glu	7.61 ± 10%	2	7.86 ± 10%	2
Gly	0.78 ± 28%	17		
GPC	1.30 ± 9%	4	1.28 ± 9%	4
GSH	1.75 ± 10%	5	1.82 ± 9%	5
Lac	1.27 ± 22%	8	1.29 ± 23%	8
mI	6.18 ± 4%	2	6.29 ± 4%	2
NAA	7.42 ± 9%	2	7.55 ± 9%	2
NAAG	1.11 ± 10%	6	1.11 ± 9%	7
PCh	0.69 ± 19%	14	0.59 ± 20%	16
PCr	5.14 ± 6%	3	5.07 ± 5%	3
PE	1.98 ± 7%	7	1.96 ± 8%	7
Tau	4.17 ± 16%	3	4.15 ± 17%	3
GPC + PCh	1.99 ± 9%	5	1.87 ± 10%	5

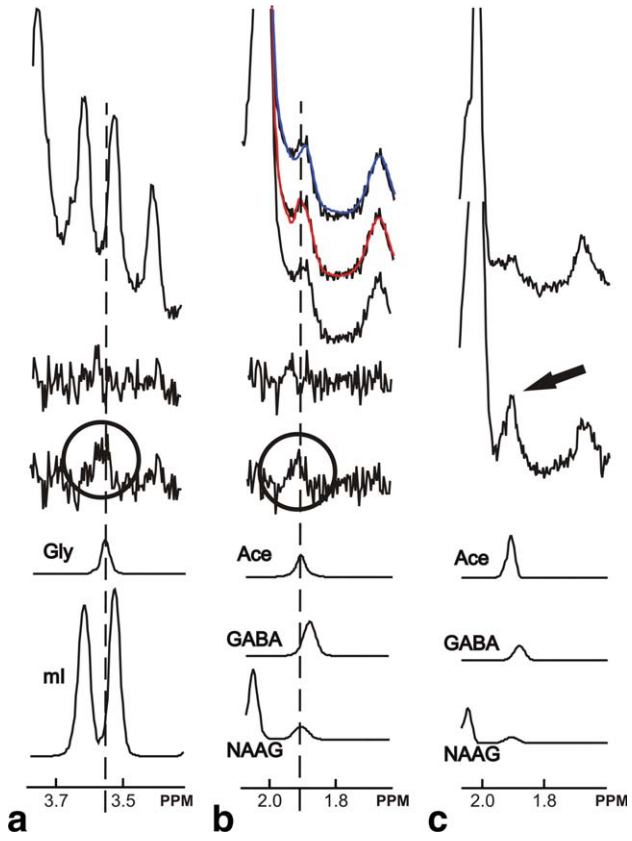

FIG. 3. Verification of the detection of Ace and Gly in the LCModel analysis. Columns **a** and **b** show the spectral regions of the Gly and the Ace peak, respectively. Shown are (from top to bottom): in vivo spectra, residuals (scaled vertically by a factor of two) with and without inclusion of Gly and Ace in the basis data, and fitting results for the examined and its overlapping metabolites. Spurious signals in the residuals are marked with circles. Column b also shows the fitted spectra without (blue line) and with (red line) including Ace in the LCModel analysis. Column **c** shows the spectra before (1st row) and during (2nd row) Ace infusion. The substantial increase of Ace is marked with an arrow. Only eddy current correction, Fourier-transformation and phase correction were applied to all spectra.

between 0.5 ppm and 2.0 ppm, where no significant residual signals remain. The alternative method of acquiring individual MM datasets for each spectrum will be difficult at high field, as assigning and eliminating residual metabolites can become a very demanding task even with the HLSVD method. The double inversion-recovery approach has been shown to reproduce the experimental baseline only poorly at 14.1 T because of the different T_1-weighting in the MM spectrum (4). These problems may be avoided with the simulation approach used in the present study. Because regional differences in MM components have been shown to have only negligible effects on quantifying metabolite concentrations (26), the parameterization performed with the metabolite-nulled spectrum from the hippocampus can be used as basis for metabolite quantification in all brain regions. This was also ascertained by obtaining metabolite-nulled spectra from thalamus, hippocampus and striatum, which did not show significant differences (data not shown).

The stable quantification of Gly was a challenging factor even with short TE at 9.4 T mainly due to the direct overlap with mI (27). To overcome this problem, several alternative approaches including the use of relatively long TE (27), TE-averaged PRESS (28), and triple refocusing pulses implemented at optimized TE (18) were reported to induce significant degradation of the mI signal while maintaining the Gly signal. In this study, Gly was resolved and quantified in all rats with average CRLB of 17%, reflecting a reliable Gly detection. The concentration was found to be 0.78 μmol/g, which is consistent with previous data from in vitro rat brain tissue extracts (29).

A prior high resolution NMR study showed that the Ace methyl resonance in PCA extracts of rat brain can be contaminated during the extraction procedure or sample storage (30). This illustrates the importance of in vivo measurements of this metabolite, which clearly avoids this problem. In this study, the Ace singlet at 1.9 ppm was detected and quantified both in the normal brain and during infusion of Ace. The Ace concentration determined as 0.52 μmol/g was in agreement with previous in vitro studies of rodent brain extracts (31,32). Excluding Ace from the basis data resulted in a slight increase of the GABA concentration by 16%. Although this is in the order of the standard deviation of the quantification, it might indicate a small overestimation of the GABA methylene resonance at 1.889 ppm when Ace is not quantified due to the overlap of these two resonances.

In conclusion, a substantial enhancement of in vivo ^{1}H NMR spectra was achieved at 16.4 T. In addition, simulated MM components showed their suitability to substitute the measured MM spectrum. Two experimentally challenging metabolites, Ace and Gly, were consistently detected with CRLB below 20%, indicating reliable quantification. These improvements will further facilitate the use of in vivo MR spectroscopy at 16.4 T to investigate neurochemical variations in the rat brain.

ACKNOWLEDGMENTS

The authors thank Drs. Stephen Provencher and Cristina Cudalbu for helpful discussions on quantification and Dr. Ivan Tkac for providing the asymmetric pulse.

REFERENCES

1. Tkac I, Rao R, Georgieff MK, Gruetter R. Developmental and regional changes in the neurochemical profile of the rat brain determined by in vivo ^{1}H NMR spectroscopy. Magn Reson Med 2003;50:24–32.
2. Pfeuffer J, Tkac I, Provencher SW, Gruetter R. Toward an in vivo neurochemical profile: quantification of 18 metabolites in short-echo-time ^{1}H NMR spectra of the rat brain. J Magn Reson 1999;141: 104–120.
3. Terpstra M, Tkac I, Rao RL, Gruetter R. Quantification of vitamin C in the rat brain in vivo using short echo-time ^{1}H MRS. Magn Reson Med 2006;55:979–983.
4. Mlynarik V, Cudalbu C, Xin L, Gruetter R. ^{1}H NMR spectroscopy of rat brain in vivo at 14.1 Tesla: improvements in quantification of the neurochemical profile. J Magn Reson 2008;194:163–168.
5. Chateil JF, Biran M, Thiaudiere E, Canioni P, Merle M. Metabolism of [1-^{13}C] glucose and [2-^{13}C] acetate in the hypoxic rat. Neurochem Int 2001;38:399–407.
6. Deelchand DK, Shestov AA, Koski DM, Ugurbil K, Henry PG. Acetate transport and utilization in the rat brain. J Neurochem 2009;109 (Suppl.1):46–54.

7. Govindaraju V, Young K, Maudsley AA. Proton NMR chemical shifts and coupling constants for brain metabolites. NMR Biomed 2000;13: 129–153.
8. Kassem MNE, Bartha R. Quantitative proton short-echo-time LASER spectroscopy of normal human white matter and hippocampus at 4 Tesla incorporating macromolecule subtraction. Magn Reson Med 2003;49:918–927.
9. Seeger U, Klose U, Mader I, Grodd W, Nagele T. Parameterized evaluation of macromolecules and lipids in proton MR Spectroscopy of brain diseases. Magn Reson Med 2003;49:19–28.
10. Pfeuffer J, Juchem C, Merkle H, Nauerth A, Logothetis NK. High-field localized ^{1}H NMR spectroscopy in the anesthetized and in the awake monkey. Magn Reson Imaging 2004;22:1361–1372.
11. Patel AB, de Graaf RA, Mason GF, Rothman DL, Shulman RG, Behar KL. The contribution of GABA to glutamate/glutamine cycling and energy metabolism in the rat cortex in vivo. Proc Natl Acad Sci U S A 2005;102:5588–5593.
12. Tkac I, Starcuk Z, Choi IY, Gruetter R. In vivo ^{1}H NMR spectroscopy of rat brain at 1 ms echo time. Magn Reson Med 1999;41: 649–656
13. Gruetter R. Automatic, localized in vivo adjustment of all first- and second-order shim coils. Magn Reson Med 1993;29:804–811.
14. Terpstra M, Gruetter R. ^{1}H NMR Detection of vitamin C in human brain in vivo. Magn Reson Med 2004;51:225–229.
15. de Graaf RA, Braun KPJ, Nicolay K. Single-shot diffusion trace ^{1}H NMR spectroscopy. Magn Reson Med 2001;45:741–748.
16. Klose W. In vivo proton spectroscopy in presence of eddy currents. Magn Reson Med 1990;14:26–30.
17. Provencher SW. Estimation of metabolite concentrations from localized in vivo proton NMR spectra. Magn Reson Med 1993;30: 672–679.
18. Choi C, Bhardwaj PP, Seres P, Kalra S, Tibbo PG, Coupland NJ. Measurement of glycine in human brain by triple refocusing 1H-MRS in vivo at 3.0T. Magn Reson Med 2008;59:59–64.
19. Ernst RR, Bodenhausen G, Wokaun A. Principles of nuclear magnetic resonance in one and two dimensions. Oxford: Oxford University Press; 1987. pp 9–17.
20. Terpstra M, Marjanska M, Henry PG, Tkac I, Gruetter R. Detection of an antioxidant profile in the human brain in vivo via double editing with MEGA-PRESS. Magn Reson Med 2006;56:1192–1199.
21. Krawczyk H, Gradowska W. Characterisation of the 1H and 13C NMR spectra of N-acetylaspartylglutamate and its detection in urine from patients with canavan disease. J Pharm Biomed Anal 2003;31: 455–463.
22. Kaiser LG, Young K, Meyerhoff DJ, Mueller SG, Matson GB. A detailed analysis of localized J-difference GABA editing: theoretical and experimental study at 4 T. NMR Biomed 2008;21:22–32.
23. Pijnappel WWF, van den Boogaart A, de Beer R, van Ormondt D. SVD-based quantification of magnetic resonance signals. J Magn Reson 1992;97:122–134.
24. Naressi A, Couturier C, Devos JM, Janssen M, Mangeat C, de Beer R, Graveron-Demilly D. Java-based graphical user interface for the MRUI quantitation package. Magn Reson Mater Phy 2001;12: 141–152.
25. Provencher SW. LCModel & LCMgui user's manual. 2010. p 137, http://s-provencher.com/pub/LCModel/manual/manual.pdf.
26. Xin L, Mlynarik V, Lei H, Gruetter R. Influence of regional macromolecular baseline on the quantification of neurochemical profile in rat brain. Proc Intl Soc Mag Reson Med 2010;18: 321.
27. Gambarota G, Xin L, Perazzolo C, Kohler I, Mlynarik V, Gruetter R. In vivo 1H NMR measurement of glycine in rat brain at 9.4 T at short echo time. Magn Reson Med 2008;60:727–731.
28. Prescot AP, deB Frederick B, Wang L, Brown J, Jensen JE, Kaufman MJ, Renshaw PF. In vivo detection of brain glycine with echo-time-averaged ^{1}H magnetic resonance spectroscopy at 4.0 T. Magn Reson Med 2006;55:681–686.
29. Shank RP, Aprison MH. The metabolism in vivo of glycine and serine in eight areas of the rat central nervous system. J Neurochem 1970;17:1461–1475.
30. Martin M, Labouesse J, Canioni P, Merle M. N-acetyl-L-aspartate and acetate ^{1}H NMR signal overlapping under mild acidic pH conditions. Magn Reson Med 1993;29:692–694.
31. Colon A, Berl S, Clarke DD. Acetylation of synaptosomal protein: effect of Na^{+}. Neurochem Res 1987;12:431–438.
32. Mathew R, Arun P, Madhavarao CN, Moffett JR, Namboodiri MAA. Progress toward acetate supplementation therapy for Canavan disease: glyceryl triacetate administration increases acetate, but not N-acetylaspartate, levels in brain. J Pharmacol Exp Ther 2005;315:297–303.